[redacted]

Copy No. 84

NASA APOLLO PROGRAM WORKING PAPER NO. 1174

TRAJECTORY INFLUENCE ON THE HEATING DISTRIBUTION AROUND THE APOLLO COMMAND MODULE

SEP 1970
RECEIVED
NASA STI FACILITY
INPUT BRANCH

N70-75891
(ACCESSION NUMBER) (THRU)
37 None
(PAGES) (CODE)
TMX-65127 (CATEGORY)
(NASA CR OR TMX OR AD NUMBER)
FACILITY FORM 602

[redacted]

[redacted]

NATIONAL AERONAUTICS AND SPACE ADMINISTRATION
MANNED SPACECRAFT CENTER
HOUSTON, TEXAS

May 26, 1965

NASA APOLLO PROGRAM WORKING PAPER NO. 1174

TRAJECTORY INFLUENCE ON THE HEATING DISTRIBUTION AROUND THE APOLLO COMMAND MODULE

Prepared By: Dorothy B. Lee
Dorothy B. Lee
AST, Aerodynamics Branch

Authorized for Distribution:

Warren Gillespie, Jr.
for Maxime A. Faget
Assistant Director for Engineering and Development

NATIONAL AERONAUTICS AND SPACE ADMINISTRATION

MANNED SPACECRAFT CENTER

HOUSTON, TEXAS

May 26, 1965

CONTENTS

Page

SUMMARY 1

INTRODUCTION 1

SYMBOLS 1

RESULTS AND DISCUSSION 2

Reentry Trajectories 2
Theoretical Heating Distribution 3
Trajectory Effect on Heating Distribution 4
Atmospheric Effect on Heating 4
Turbulent Heating Comparison with Laminar Heating 4
Single Mission as Heat Shield Qualifying Trajectory 5
Comparison of NAA Trajectories with MIT Guided Trajectories . . . 6

CONCLUDING REMARKS 6

REFERENCES 8

FIGURES

Figure		Page
1	MIT guided entry trajectories	9
2	A sketch of the Apollo command module. All dimensions are in inches	10
3	Angle of attack variation of convective heating around pitch plane of Apollo command module	11
4	Distribution of radiative heating to the Apollo command module	12
5	Distribution of maximum heat rates around the pitch plane of the Apollo command module	
	(a) Shallow entry	13
	(b) Steep entry	14
	(c) 20G emergency entry	15
6	Distribution of heat load in the pitch plane of the Apollo command module	
	(a) Shallow entry	16
	(b) Steep entry	17
	(c) 20G emergency entry	18
7	Atmosphere effect on heating	
	(a) Comparison of maximum heating rates	19
	(b) Comparison of heat loads	20
8	Local Reynolds number on the Apollo command module for steep entry	
	(a) On blunt face	21
	(b) On conical section	22
9	Local Reynolds number on Apollo command module for shallow entry	
	(a) On blunt face	23
	(b) On conical section	24
10	Distribution of total heat load in the pitch plane of Apollo command module	25

Figure		Page
11	Distribution of maximum total heating rates across blunt face	26
12	Laminar distribution of total heat load across blunt face	27
13	Free-stream Reynolds numbers and stagnation-point heating rates calculated for heat shield qualification trajectory	
	(a) Free-stream Reynolds number based on body diameter	28
	(b) Stagnation-point heating rates	28
14	Comparison of NAA trajectories with MSC trajectories using MIT guidance	
	(a) Shallow entry	29
	(b) 20G emergency entry	30
15	Time histories of maximum heating rates for NAA and MSC trajectories	
	(a) Shallow entry	31
	(b) 20G emergency entry	32

TRAJECTORY INFLUENCE ON THE HEATING DISTRIBUTION AROUND THE APOLLO COMMAND MODULE

By Dorothy B. Lee

SUMMARY

The effects of lift-to-drag ratio, entry angle, atmosphere and type of boundary-layer flow on the distribution of heating rates to the Apollo command module are discussed and comparisons of the effect of varying these parameters are presented. It is shown that the entry angle has the greatest influence on the location on the blunt face of the maximum heat load. A large effect of lift-to-drag change and atmospheric deviation is indicated.

INTRODUCTION

Since the trajectory of a vehicle entering the earth's atmosphere from a lunar mission dictates the thickness of the heat shield material, much study has gone into the development of heat shield design trajectories for the Apollo command module. The present design limits for the entry trajectory and heat shield performance are based on lift-to-drag ratios (L/D) of .3 to .4, initial entry angles of -5.20° to -9.45° and on a non-standard atmosphere given in reference 1. The purpose of this paper is to show the influence of various trajectory parameters on the heating estimates to the command module and how they affect the distribution of the heating around the entry configuration.

SYMBOLS

D	maximum body diameter, 12.833 ft
G	load factor
L/D	lift-to-drag ratio

q	heating rate, Btu/ft^2/sec
Q	total heating, Btu/ft^2
R	maximum body radius, 6.4167 ft
$R_{\infty,D}$	free-stream Reynolds number based on body diameter
$R_{l,x}$	local Reynolds number based on distance from the stagnation point
S	distance along surface from center of spherical heat shield, ft
t	time, sec
V	velocity, ft/sec
x	distance along surface from stagnation point, ft
α	angle of attack, deg
γ	flight path angle, deg
μ	absolute viscosity, slugs/ft/sec
ρ	density, slugs/ft^3

Subscripts:

D	diameter
t	stagnation
total	convective plus radiative
l	local
∞	free-stream

RESULTS AND DISCUSSION

Reentry Trajectories

The MIT guidance logic that is planned for the Apollo reentry vehicle has been programed in the IBM 7040 digital computer by the

Atmospheric Entry Guidance Group of the Guidance and Control Division. The initial conditions of flight path angle, ballistic number corresponding to L/D, range target and roll angle have been varied in the attempt to determine the most critical heat shield design trajectories. The various trajectories are shown in figure 1. The steepest entry angle studied (-9.45°) is not shown for L/D = .3 since it exceeds the 20G limit imposed on the structural design. The shallow entries (γ = -5.2°) were computed with the use of the non-standard atmosphere (ref. 1) identified as the January atmosphere which includes a density deviation from the U.S. Standard Atmosphere, 1962 (ref. 2). The steep entries were run with the 1962 standard atmosphere since the density deviation is ineffective for the relatively short reentry time. Also, the maximum heating rate occurs after the January density becomes less than the standard density.

Theoretical Heating Distribution

The convective heating rates on the Apollo command module (fig. 2), computed for this study, are based on smooth body measurements obtained in wind tunnel tests referenced to a measured zero angle of attack stagnation-point rate. Figure 3 shows the measured angle of attack variation of the convective distribution in the pitch plane of the Apollo command module. The local convective heating rates were calculated with the use of figure 3 and the curve fit equation of the stagnation point theory (ref. 3). The effect of protuberances was not included in the calculations. The computer program calculates the heating rates for the location on the blunt reentry face at S/R = .9875 since the original angle of attack computations (α = 33°, L/D = .5) found this to be the maximum heating location (ref. 4). The decrease in L/D, currently .3 and .4, has resulted in a shift of the maximum heating location which will be discussed later.

The radiative heating rates to the flight angle-of-attack stagnation point have been calculated as described in reference 5 and tabulated as functions of altitude and velocity for the computer program table lookup. The values include non-equilibrium, equilibrium and ultraviolet radiation based on standard atmospheric conditions (ref. 2). In order to obtain the radiative heating at S/R = .9875, the stagnation-point radiative heating rates were multiplied by 0.53 for L/D = .4 and 0.49 for L/D = .3 as shown by the distribution curves given in figure 4. The angle of attack corresponding to L/D used in this study is α = 20° for L/D = .3 and 25° for L/D = .4. The location of the stagnation point for various angles of attack was obtained from pressure measurements made in tunnel tests. When α = 20° the stagnation point is approximately at S/R = .65 and when α = 25° at S/R = .75.

Trajectory Effect on Heating Distribution

The maximum heating rates anticipated across the entry face of the Apollo command module at angle of attack are presented in figure 5 to illustrate the effect that L/D and the reentry angle have on the heating distribution. The values were computed for the time the summation of convective plus radiative rates at S/R = .9875 reach a peak during entry from the trajectories shown in figure 1. Examination of figure 5 reveals the shifting of the maximum heating rate location with the L/D change and the shaping of the distribution with entry angle change. The maximum heating location moves toward the center of the heat shield near the stagnation point as the L/D decreases.

The effect of L/D and entry angle on the heat load is illustrated in figure 6. The L/D change from .4 to .3 increases the heat load between 5 percent and 22 percent across the blunt face during the shallow entry and about 10 percent on the leeward half of the blunt face during the steep entry. On the other hand, the change from .4 to .3 decreases the heat load near the stagnation point during the steep entry by as much as 13 percent. The effect of the entry angle can be seen by comparing figure 6(a) with 6(b) and 6(c). The shallow angle results in the convective distribution dictating the location of the maximum total heat load which occurs at S/R = .9875 while the steeper angles shift the peak toward the center of the blunt face due to the radiative distribution having a greater influence.

Atmospheric Effect on Heating

The effect of a non-standard atmosphere on the heating is demonstrated in figure 7. Comparison of the maximum heating rates and loads shows that the standard atmosphere yields higher rates (fig. 7(a)) while the January deviation (ref. 1) from standard produces higher heat loads (fig. 7(b)). Approximately 24 percent higher heat load across the blunt face was obtained with the use of the January deviation. Thus, it can be seen that the atmospheric deviation has a significant influence on the magnitude of the total heat load.

Turbulent Heating Comparison with Laminar Heating

As turbulent flow is more likely to occur during the steep entries, a study was made of the influence turbulent flow may have on the total heat load during a 20G emergency entry. Several locations on the Apollo command module were investigated and time histories of the local Reynolds numbers for six of the locations are shown in figure 8. The length used for the Reynolds number is taken from the stagnation point. The local conditions were computed from stagnation conditions behind a normal shock

expanded isentropically to the local pressures obtained from wind tunnel test correlations and the use of the charts of reference 6. The free-stream Reynolds number based on body diameter peaks at 3.18×10^6 during the early portion of the entry trajectory and reaches a value of 2.64×10^6 at 600 seconds.

The assumption of a transition Reynolds number of $.15 \times 10^6$, a value consistent with results found in reference 7, indicates that transition is likely to occur on the blunt face during steep entries (fig. 8(a)) but not until late in the flight on the windward conical section (fig. 8(b)). Since transition was observed at a Reynolds number of 20 000 in a separated region on the Mercury spacecraft conical section (ref. 8), transition could begin early in flight on the leeward conical section of the Apollo configuration (fig. 8(b), S/R = -1.468) which will also be in separated flow.

Reynolds numbers calculated for the shallow entry were found to be an order of magnitude lower than those of the steep reentry. Figure 9 shows the time histories of the local Reynolds numbers computed at the same locations as shown in figure 8. Based on the above assumptions, transition will not occur until very late during the shallow entry on either the blunt face or the conical section.

The determination of transition Reynolds number remains a nebulous feat which suggests consideration of possible levels of turbulent heating. The theory of reference 9 was used for the turbulent study with transition beginning at the Reynolds number at which the turbulent skin friction coefficient exceeds the laminar value ($R_{l,x}$ = 15 000). The reference length used in the turbulent calculations is the distance from the stagnation point to the location considered. Distributions of total heat loads are given in figure 10 to illustrate the turbulent increase over the laminar for the steep entry and how it compares with the laminar loads for the shallow entries. As can be seen in figure 10 the turbulent calculations, designated with circular symbols, do not exceed the shallow entry heat loads for the L/D = .3 trajectory but do exceed those of the L/D .4 shallow entry.

Single Mission as Heat Shield Qualifying Trajectory

Two flight tests were considered originally to qualify the Apollo heat shield for manned missions. One trajectory was to provide the high heat rates (steep entry) while another was to yield high heat loads (shallow entry). A single trajectory has been proposed for qualification of the heat shield having an entry angle of -7.13° and a 9G acceleration. The calculated heating rates and loads for this trajectory are compared

in figures 11 and 12, respectively, with those of the two originally planned entry tests. The maximum total heating rate computed for the proposed trajectory is 60 percent of the value calculated for the steep entry test. The total heat load anticipated for the proposed trajectory is within 68 percent of the shallow entry trajectory. Time histories of the stagnation-point heating rates are shown in figure 13 along with the free-stream Reynolds number based on body diameter of 12.833 feet.

Comparison of NAA Trajectories with MIT Guided Trajectories

As a matter of interest, a comparison of the design trajectories that have evolved over the past two years is shown in figure 14. The development of Program Apollo has brought about revisions of command module weight and L/D estimates that make the original trajectories computed by NAA inapplicable for heat shield design. The NAA trajectories were based on a lighter weight command module with a trim L/D of .5 modulated by roll about the velocity vector. The heat shield design trajectories are now based on the latest MIT guidance equations with a heavier command module at L/D's between .3 and .4. The NAA shallow entry ($\gamma = -5.5^{\circ}$) takes approximately 1500 seconds to traverse the atmosphere from 400×10^3 to 100×10^3 feet altitude while the MIT guided trajectories take 950 seconds to travel the same altitude change. In contrast, the NAA 20G reentry takes only 130 seconds to reach 100×10^3 feet while MIT steep entries require 400 to 600 seconds. The roll program employed by NAA keeps the trajectory in the atmosphere throughout reentry but the MIT trajectories skip to attitudes between 250 000 and 400 000 feet.

The difference between the NAA and MIT guided entries is reflected in the heating. Comparisons of the total heating rates that occur at the locations of maximum heating for the two types of trajectories are shown in figure 15. The maximum heating locations are the stagnation points for the MIT trajectories and near the corner at S/R = .9875 for the NAA trajectories. Listed on the figure are the total heat loads, Q_{total} (Btu/ft^2), of the corresponding heat rate histories. The NAA heating values are based on a relative velocity obtained by subtracting 1160 ft/sec from the inertial velocity supplied by NAA.

CONCLUDING REMARKS

A study has been made of the effects of L/D, entry angle, atmosphere and type of boundary-layer flow on the heating to the Apollo command module. These parameters were varied in an attempt to determine

the most critical trajectories and the following observations can be made:

a. As the L/D is decreased, the maximum heat load location on the blunt entry face shifts toward the flight stagnation point.

b. The initial entry angle greatly influences the location of the maximum heat load on the entry face. The maximum total heat load is located near the corner at S/R = .9875 for the shallow entry but moves to the stagnation region for the steep entry due to the radiative distribution having a greater influence than the convective component. This trend has been observed with all MTT guided trajectories computed at L/D values between .3 and .4.

c. Use of the January deviation of density from the U.S. Standard atmosphere increases the heat load as much as 24 percent over the use of the 1962 U.S. Standard for shallow entries ($\gamma = -5.2°$). No effect of the January atmosphere was noted on the steep entries.

REFERENCES

1. Cole, A. E., and Kantor, A. J.: Air Force Interim Supplemental Atmosphere to 90 Kilometers. Air Force Surveys in Geophysics no. 153, Dec. 1963.

2. U.S. Standard Atmosphere, 1962. NASA USAF, Weather Bureau, 1962.

3. Detra, R. W., Kemp, N. H., and Riddell, F. R.: Addendum to Heat Transfer to Satellite Vehicles Reentering the Atmosphere. Jet Propulsion, vol. 27, no. 12, Dec. 1957, pp. 1256-1257.

4. Lee, Dorothy B., Bertin, John J., and Ried, Robert C., Jr.: Apollo Reentry Heating. NASA Program Apollo Working Paper 1089, Sept. 13, 1963.

5. Ried, Robert C., Jr., Lee, Dorothy B., and Willis, Noel C., Jr.: Stagnation Point Radiative Heating Estimates for Blunt Reentry Vehicles. MSC Internal Note no. 64-ET-64. Sept. 1964.

6. Moeckel, W. E., and Weston, Kenneth C.: Composition and Thermodynamic Properties of Air in Chemical Equilibrium. NACA TN 4265 Apr. 1958.

7. Bertin, John J.: Wind-Tunnel Heating Rates for the Apollo Spacecraft. NASA TM X-1033. Jan. 1965.

8. Weston, Kenneth C., and Fitzkee, Archie L.: Afterbody Heat Transfer Measurements Obtained During Reentry of the Spacecraft of the Mercury-Atlas 5 Mission. NASA TM X-564. Dec. 1963.

9. Van Driest, E. R.: On Skin Friction and Heat Transfer Near the Stagnation Point. NAA, Inc. AL-2267, Mar. 1956.

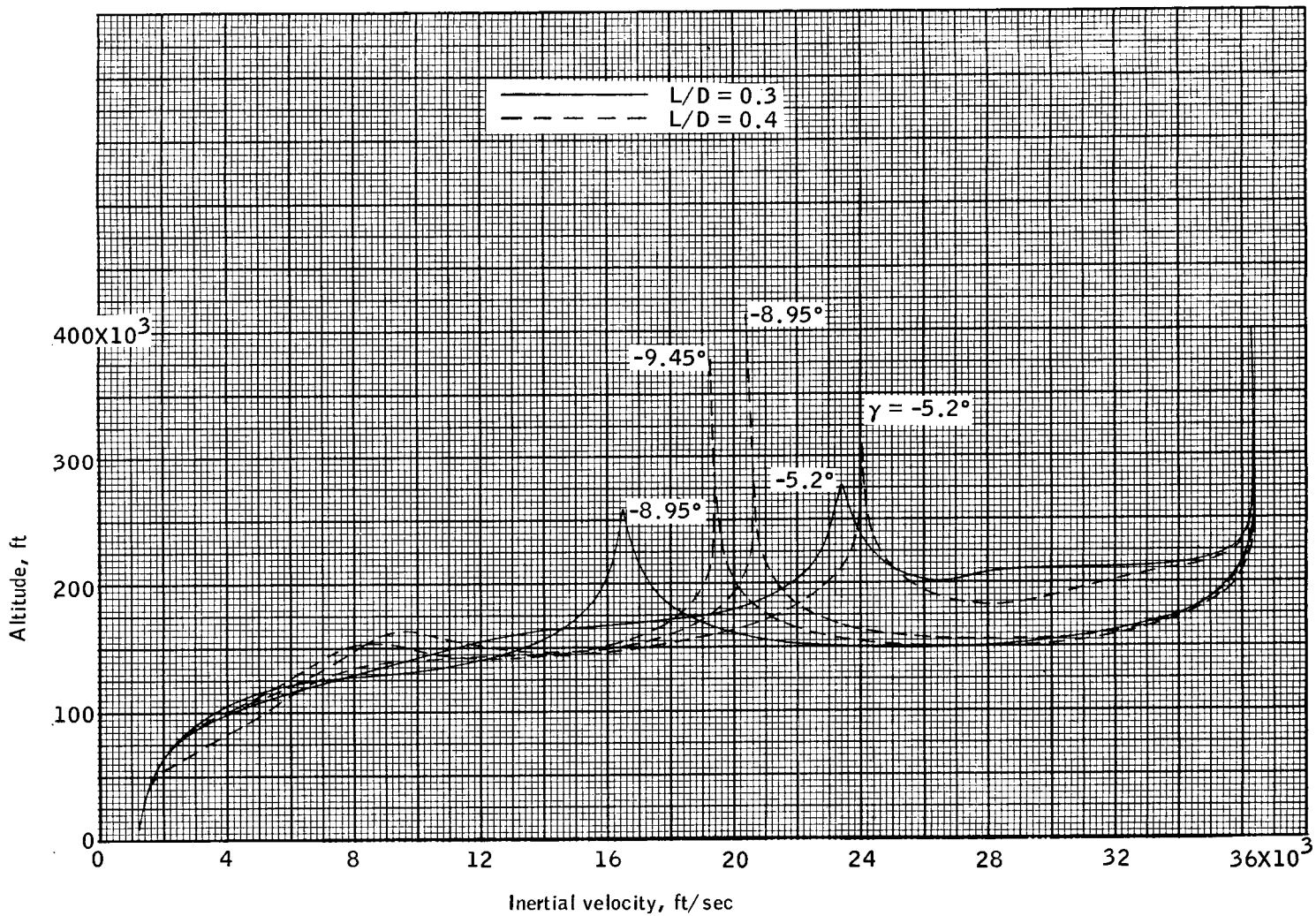

Figure 1.- MIT guided entry trajectories.

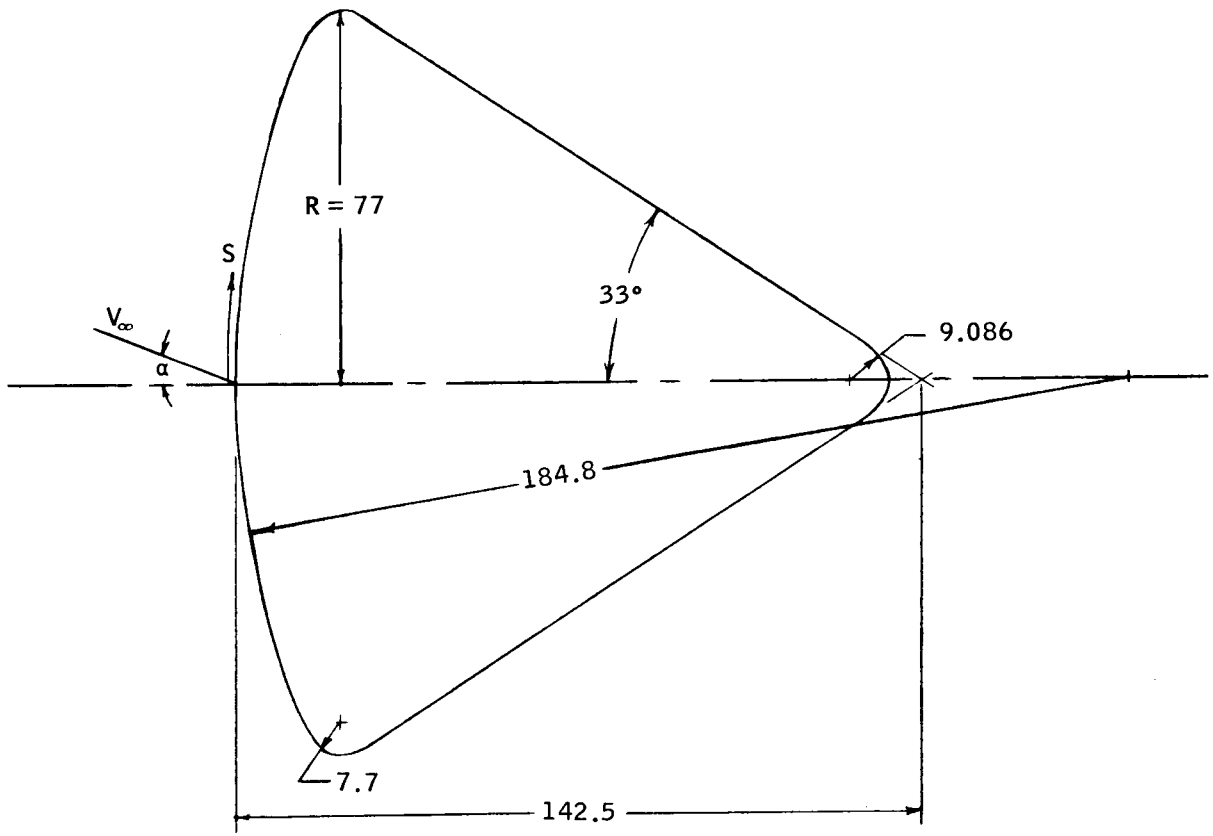

Figure 2.- A sketch of the Apollo command module. All dimensions are in inches.

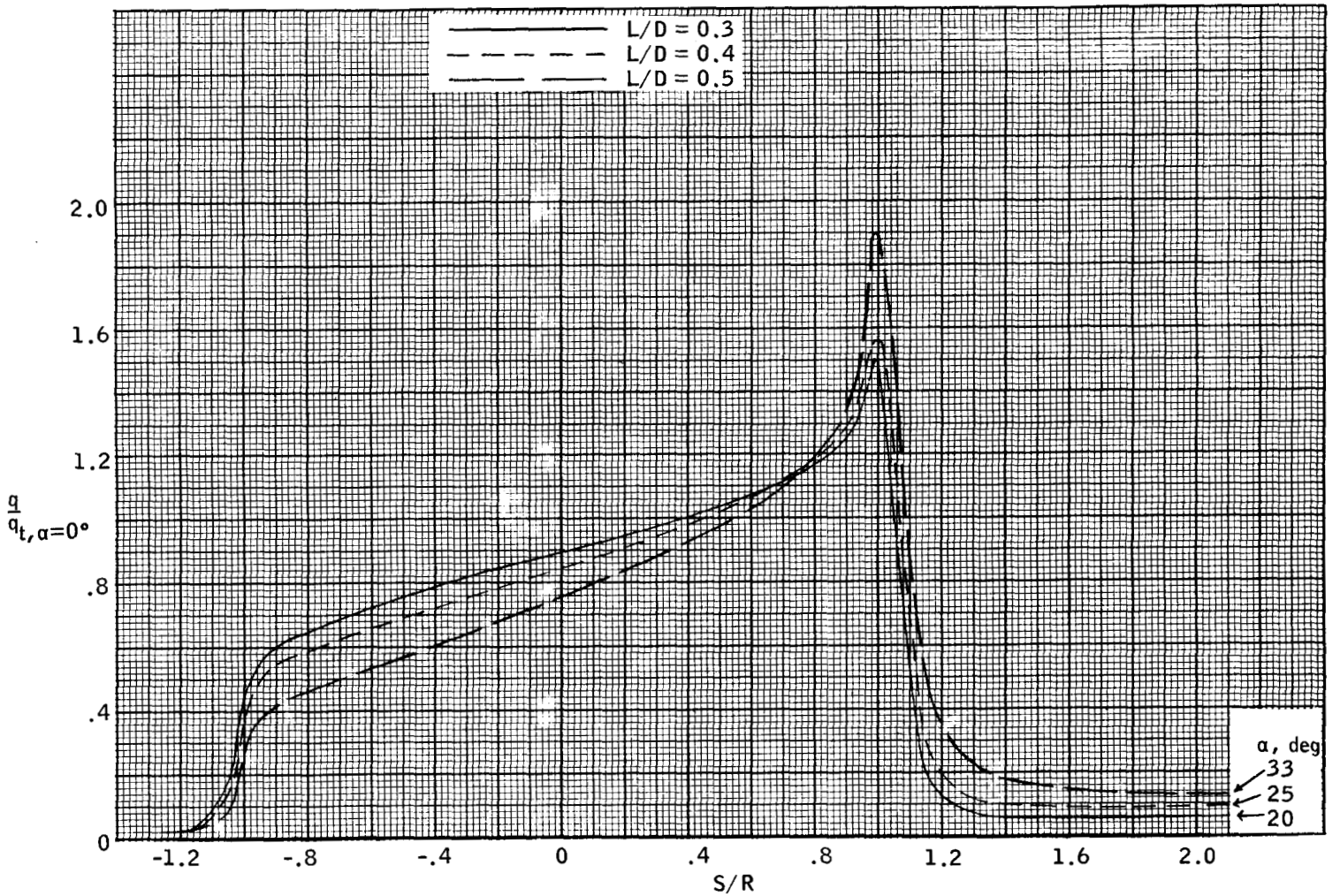

Figure 3.- Angle of attack variation of convective heating around pitch plane of Apollo command module.

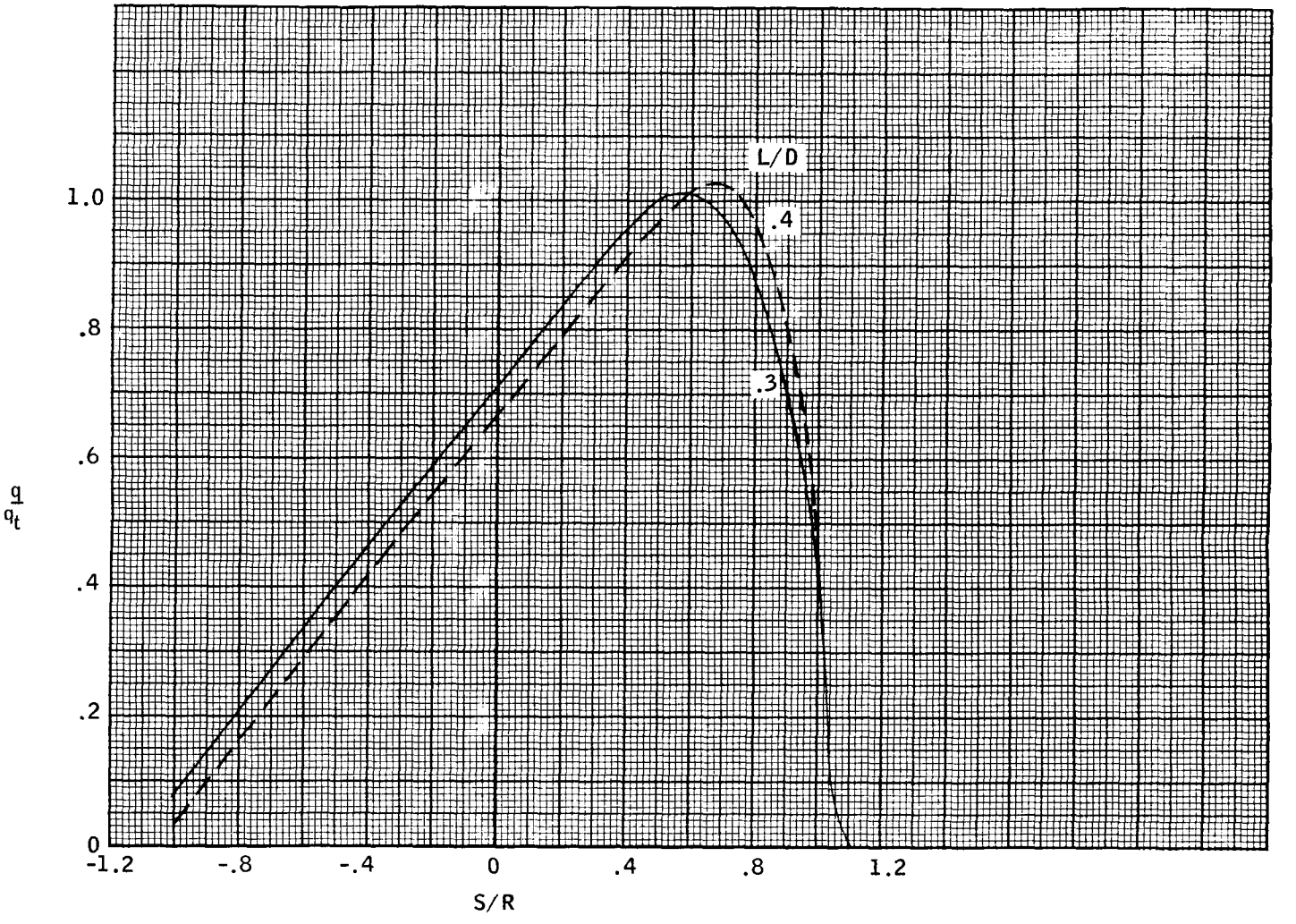

Figure 4.- Distribution of radiative heating to the Apollo command module.

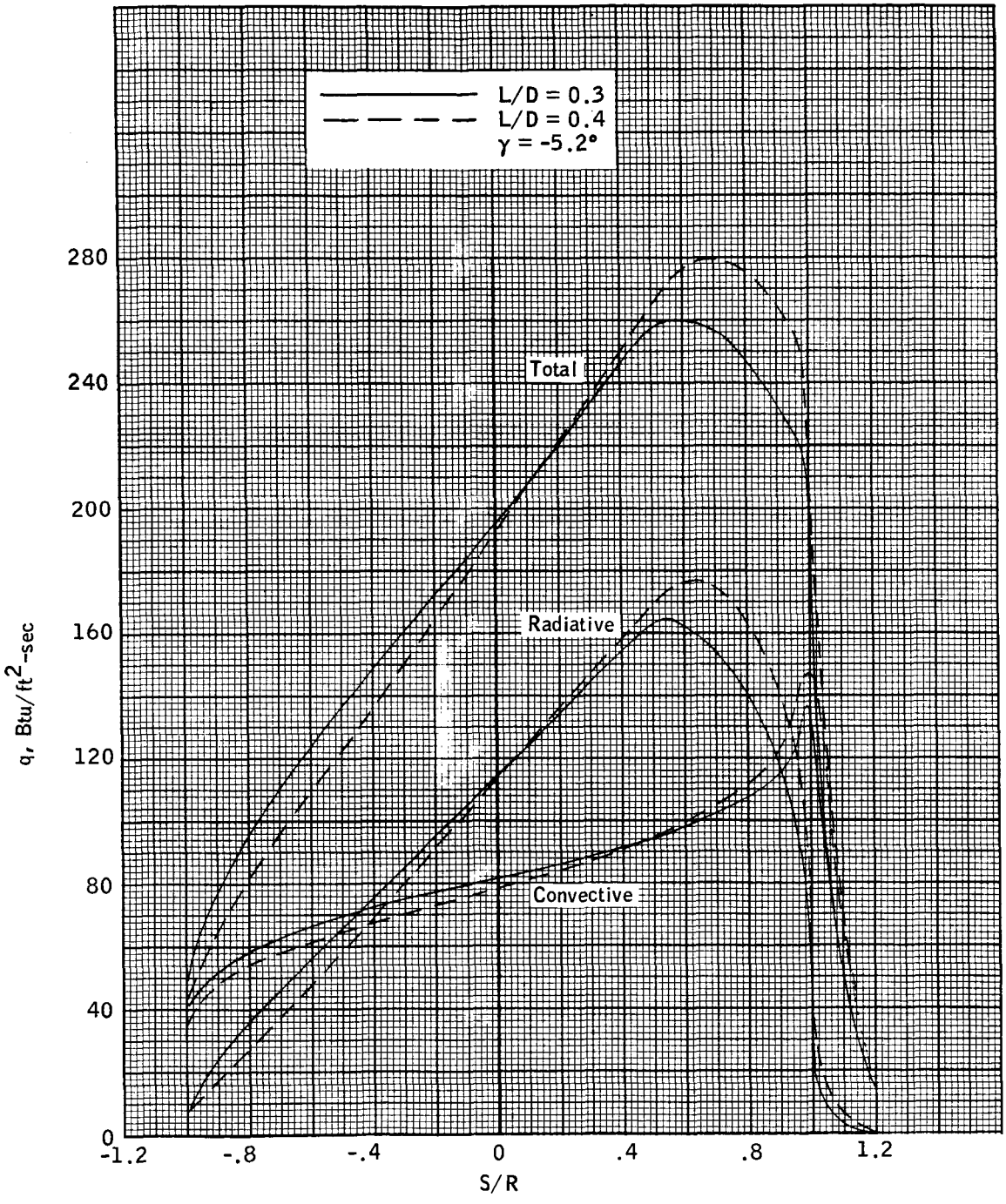

(a) Shallow entry.

Figure 5.- Distribution of maximum heat rates around the pitch plane of the Apollo command module.

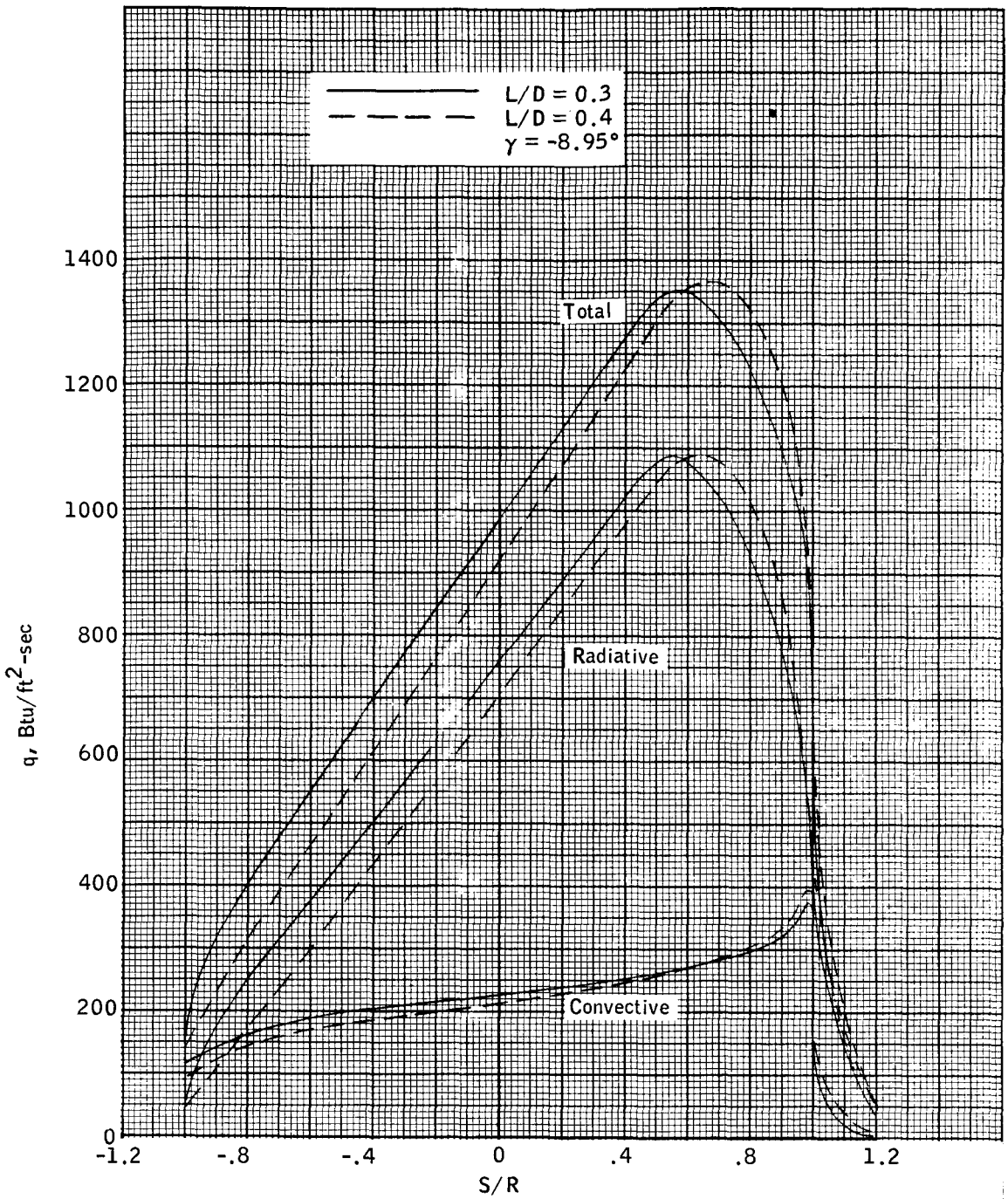

(b) Steep entry.

Figure 5.- Continued.

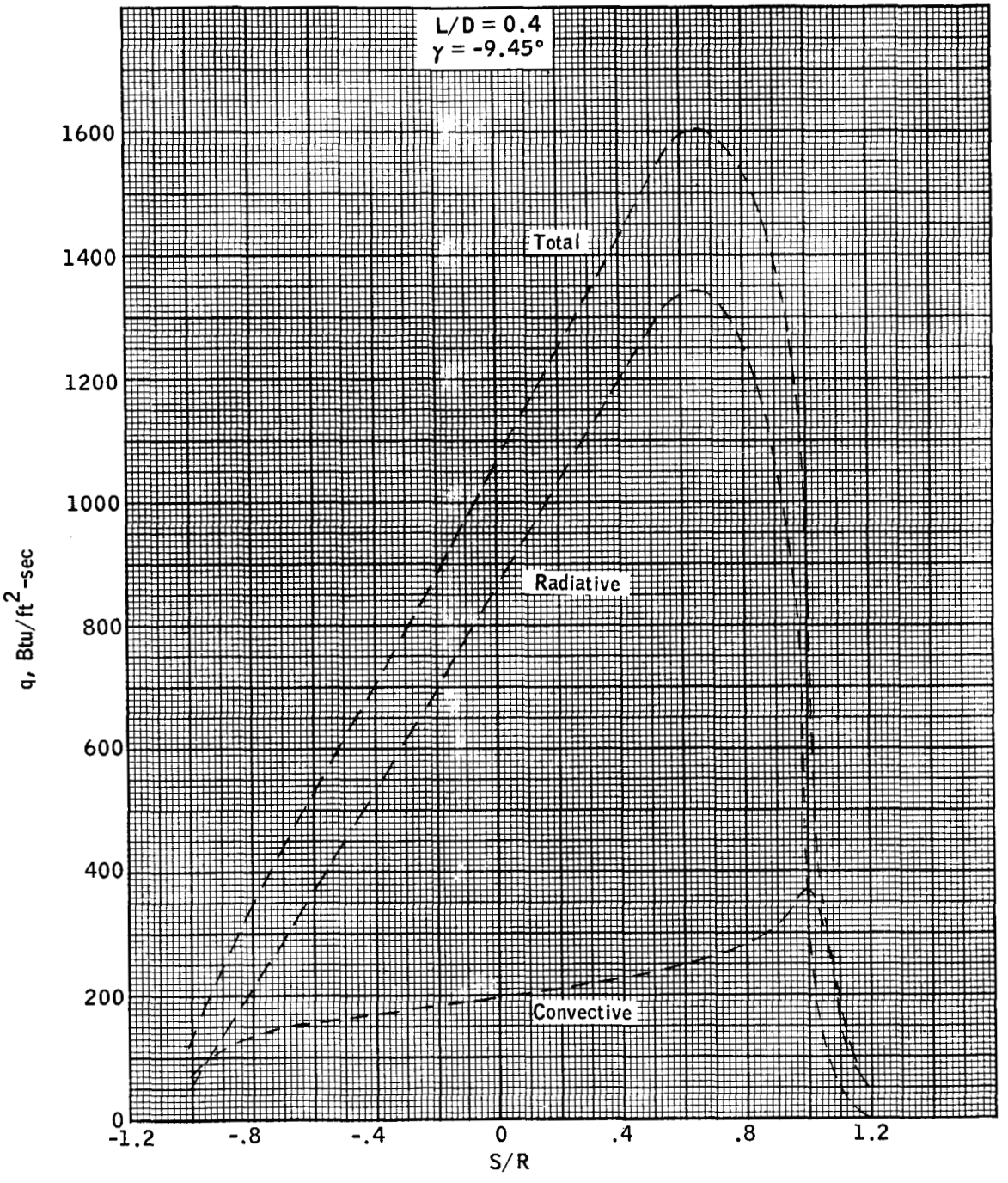

(c) 20 G emergency entry.

Figure 5.- Concluded.

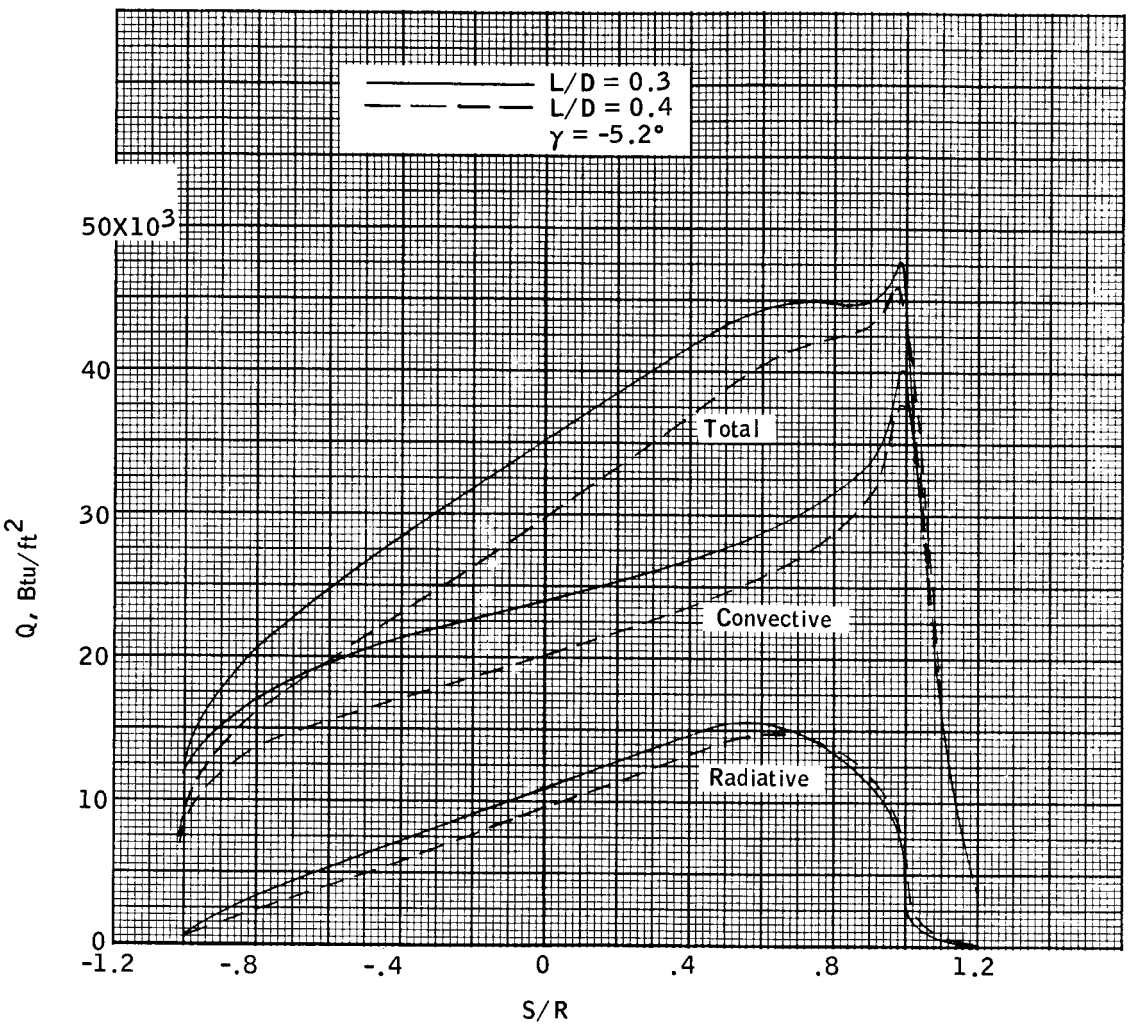

(a) Shallow entry.

Figure 6.- Distribution of heat load in the pitch plane of the Apollo command module.

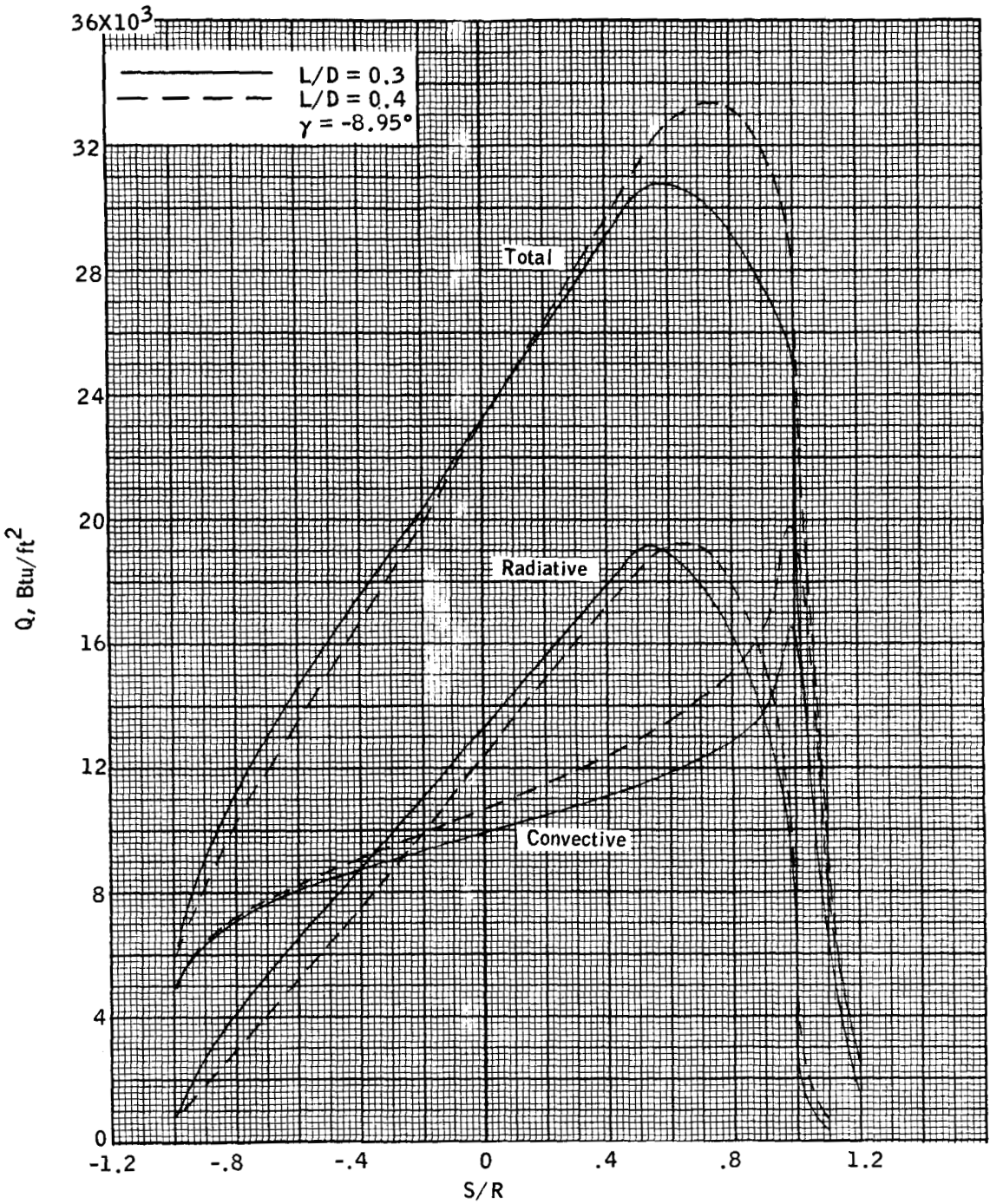

(b) Steep entry.

Figure 6.- Continued.

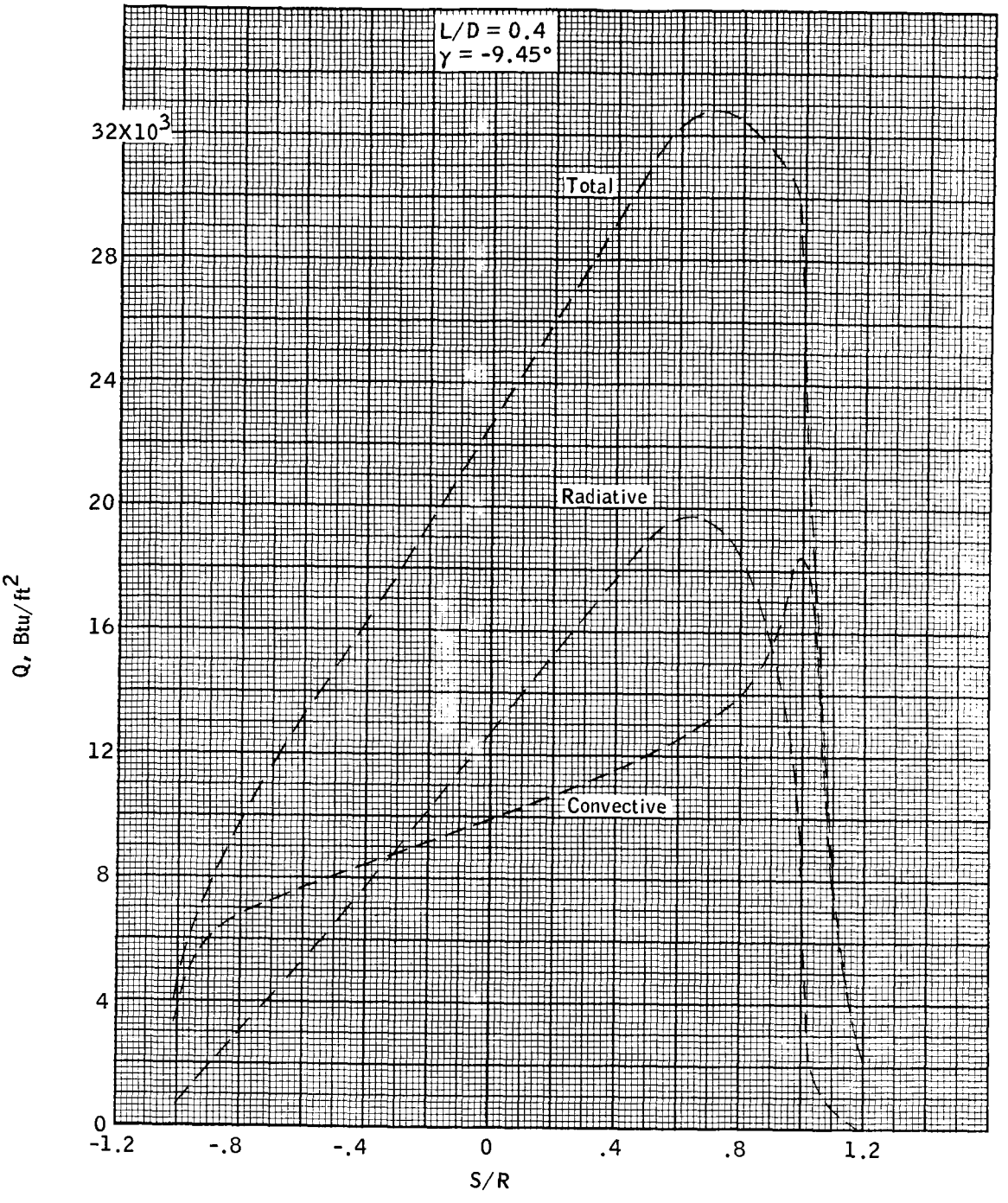

(c) 20 G emergency entry.

Figure 6.- Concluded.

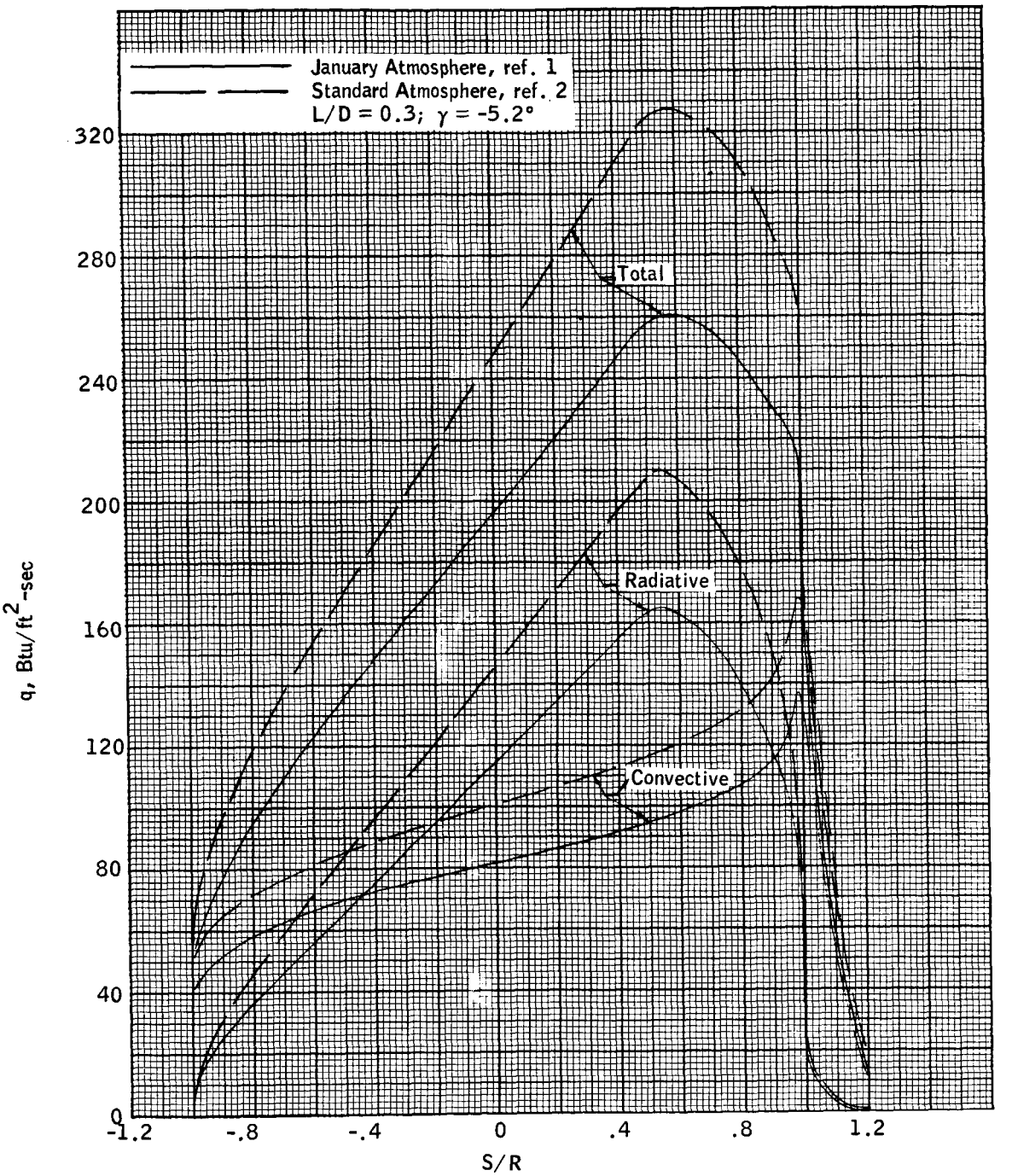

(a) Comparison of maximum heating rates.

Figure 7.- Atmosphere effect on heating.

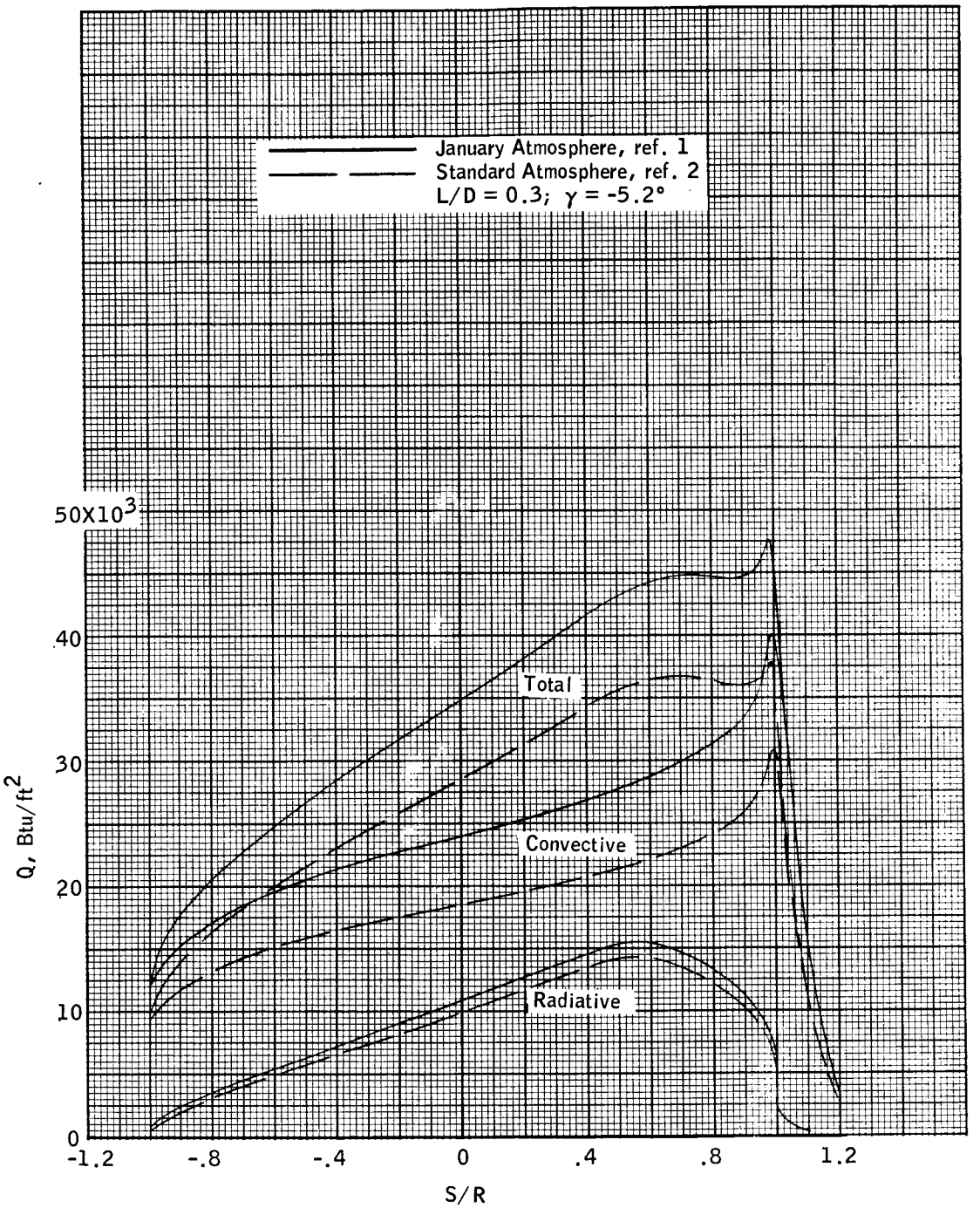

(b) Comparison of heat loads.

Figure 7.- Concluded.

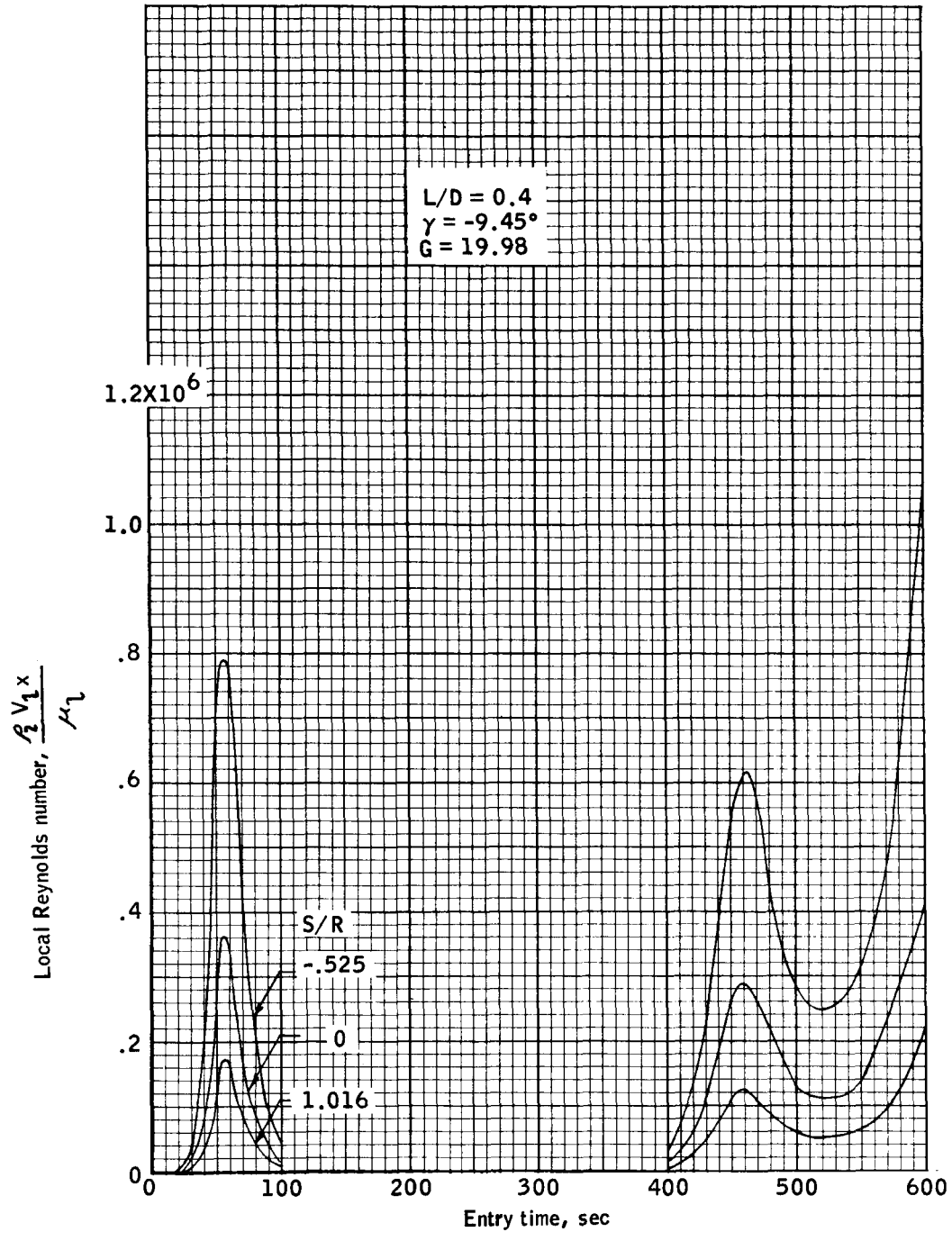

(a) On blunt face.

Figure 8.- Local Reynolds number on the Apollo command module for steep entry.

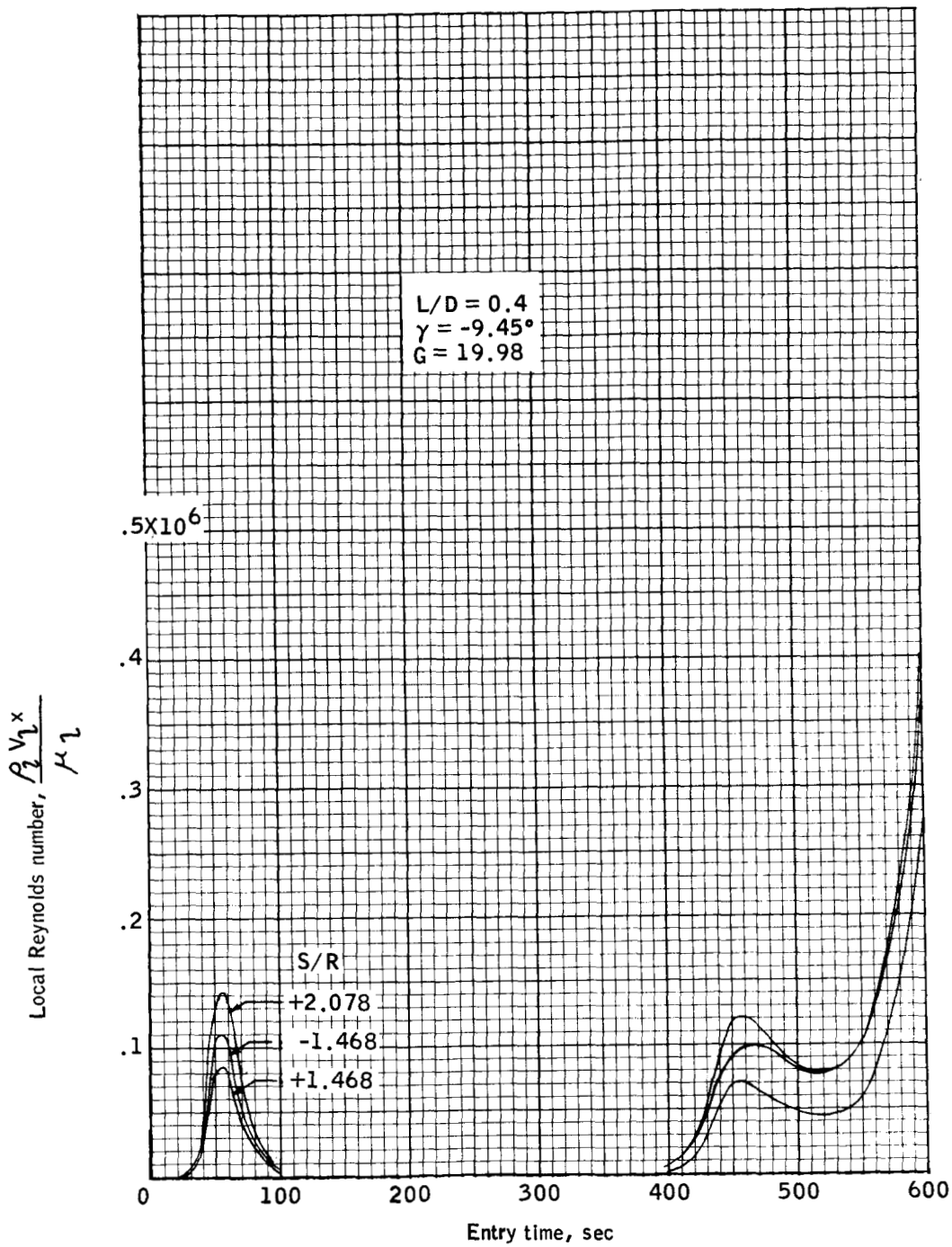

(b) On conical section.

Figure 8.- Concluded.

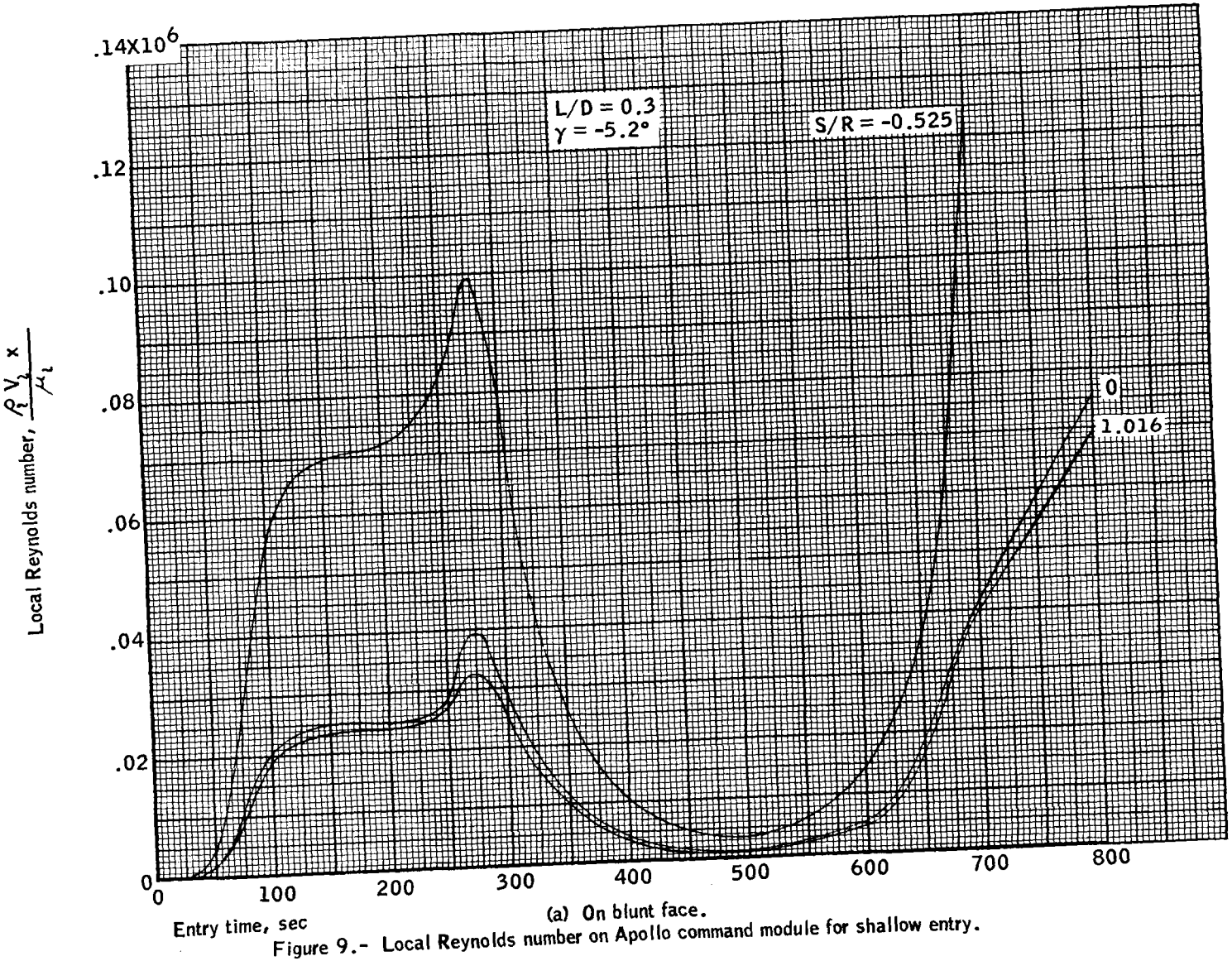

(a) On blunt face.

Figure 9.- Local Reynolds number on Apollo command module for shallow entry.

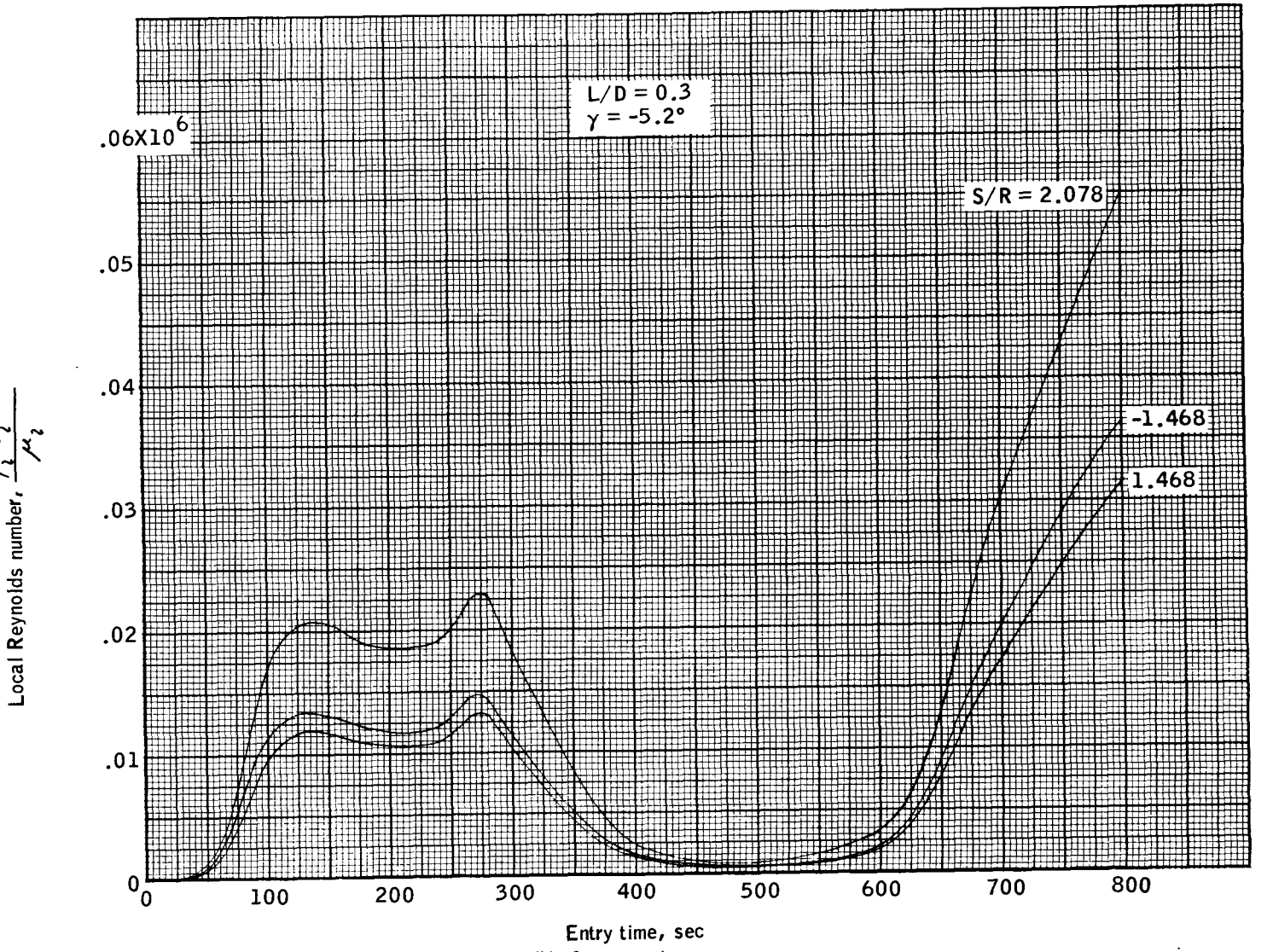

(b) On conical section.
Figure 9.- Concluded.

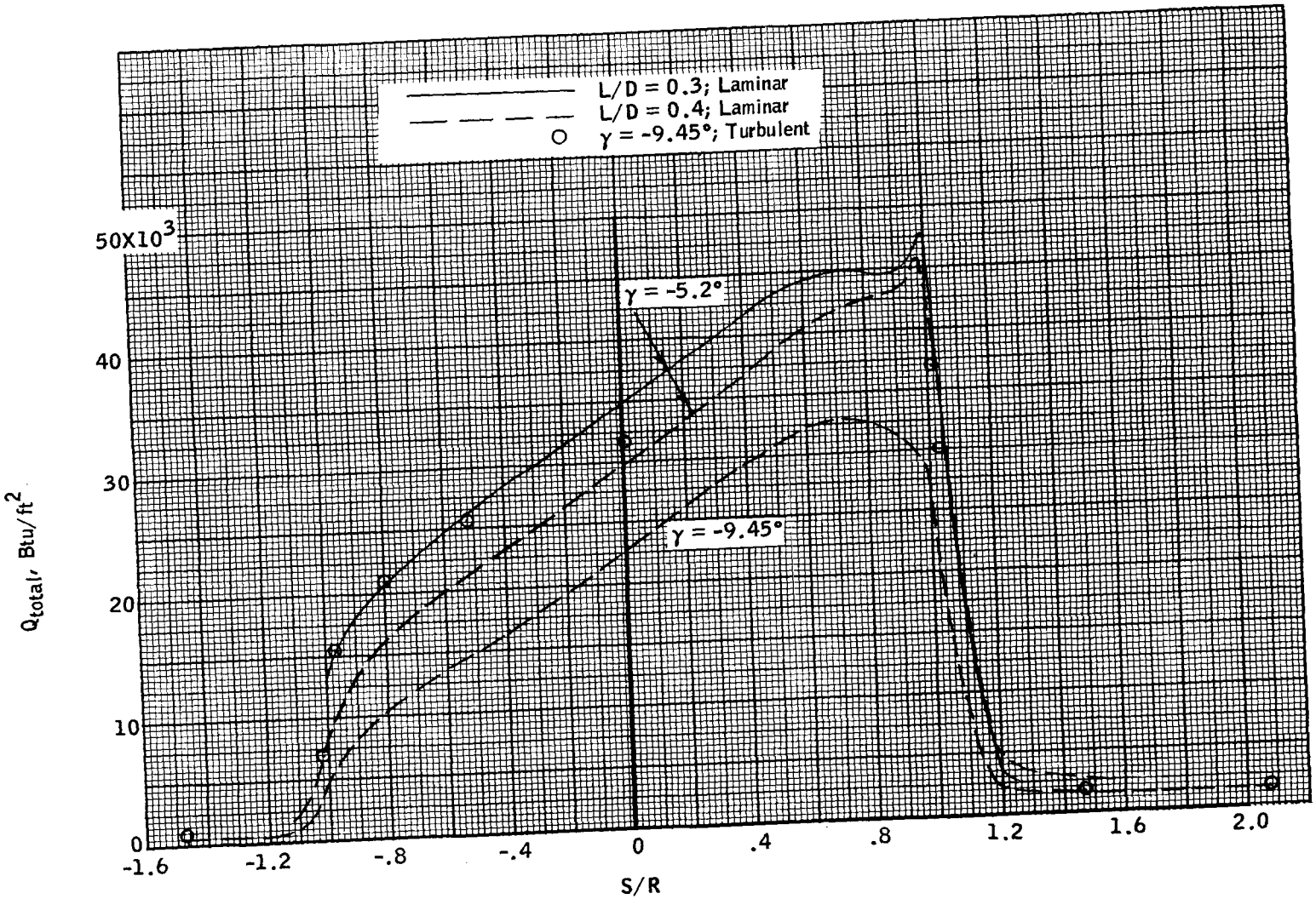

Figure 10.- Distribution of total heat load in the pitch plane of Apollo command module.

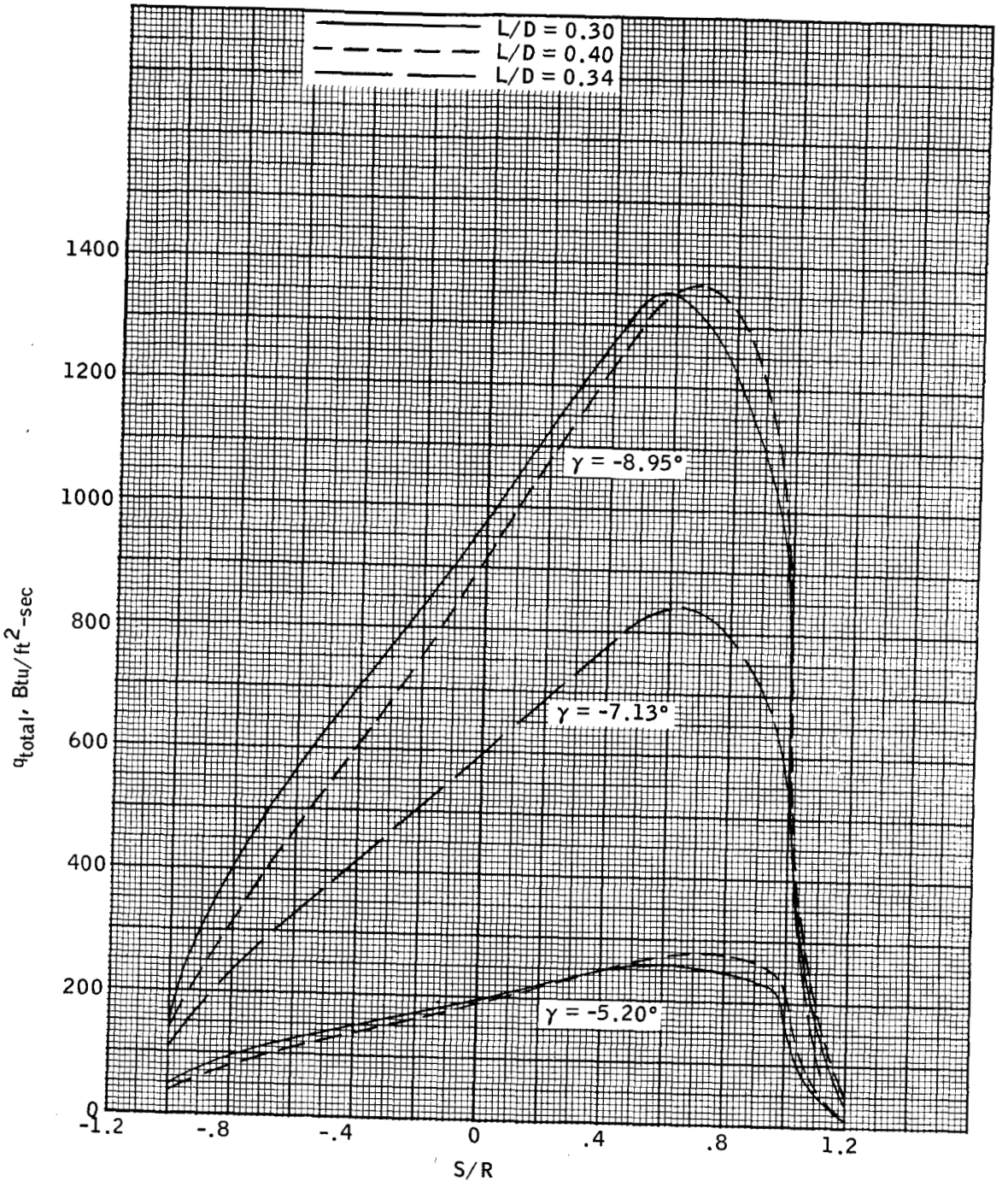

Figure 11.- Distribution of maximum total heating rates across blunt face.

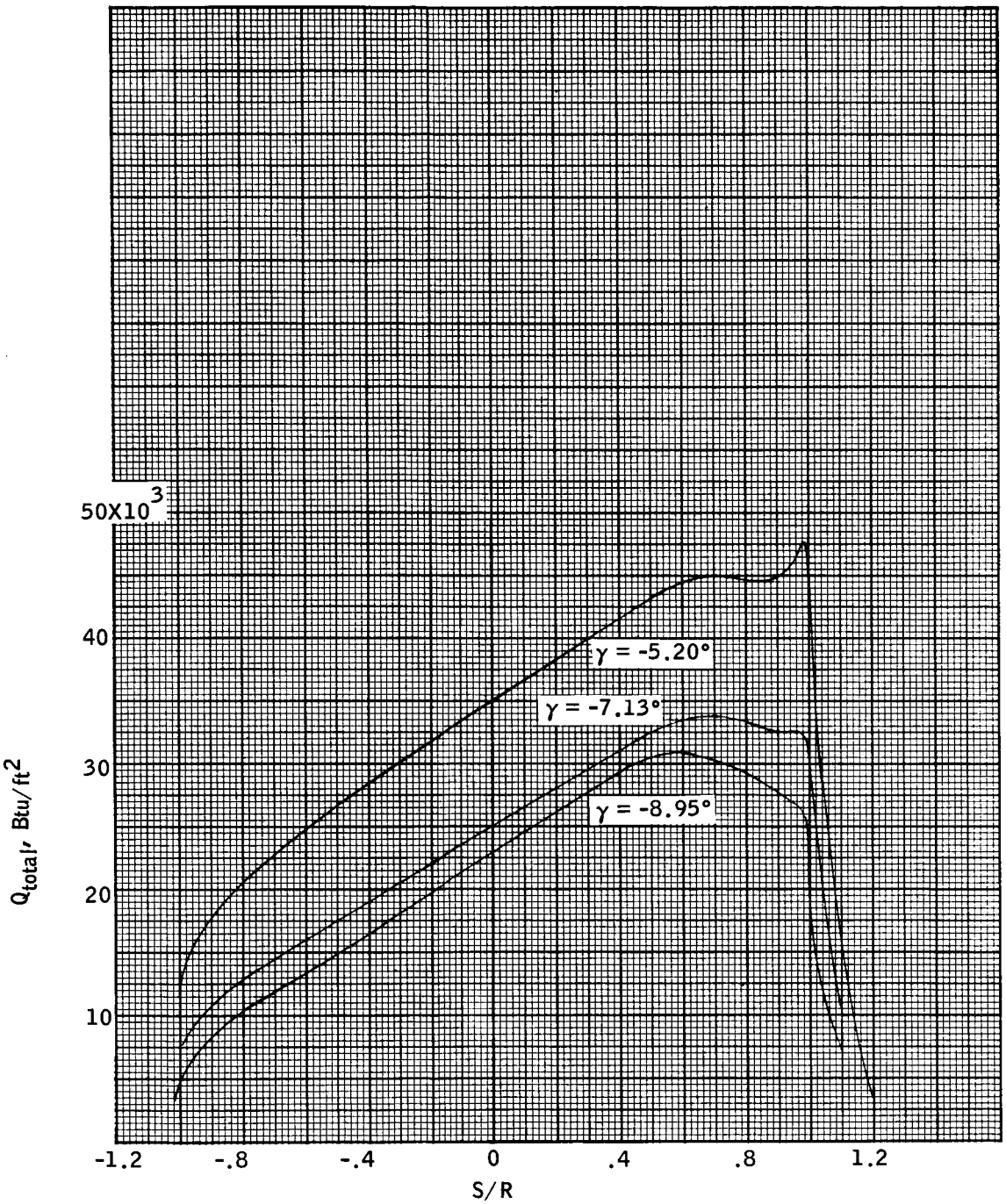

Figure 12.- Laminar distribution of total heat load across blunt face.

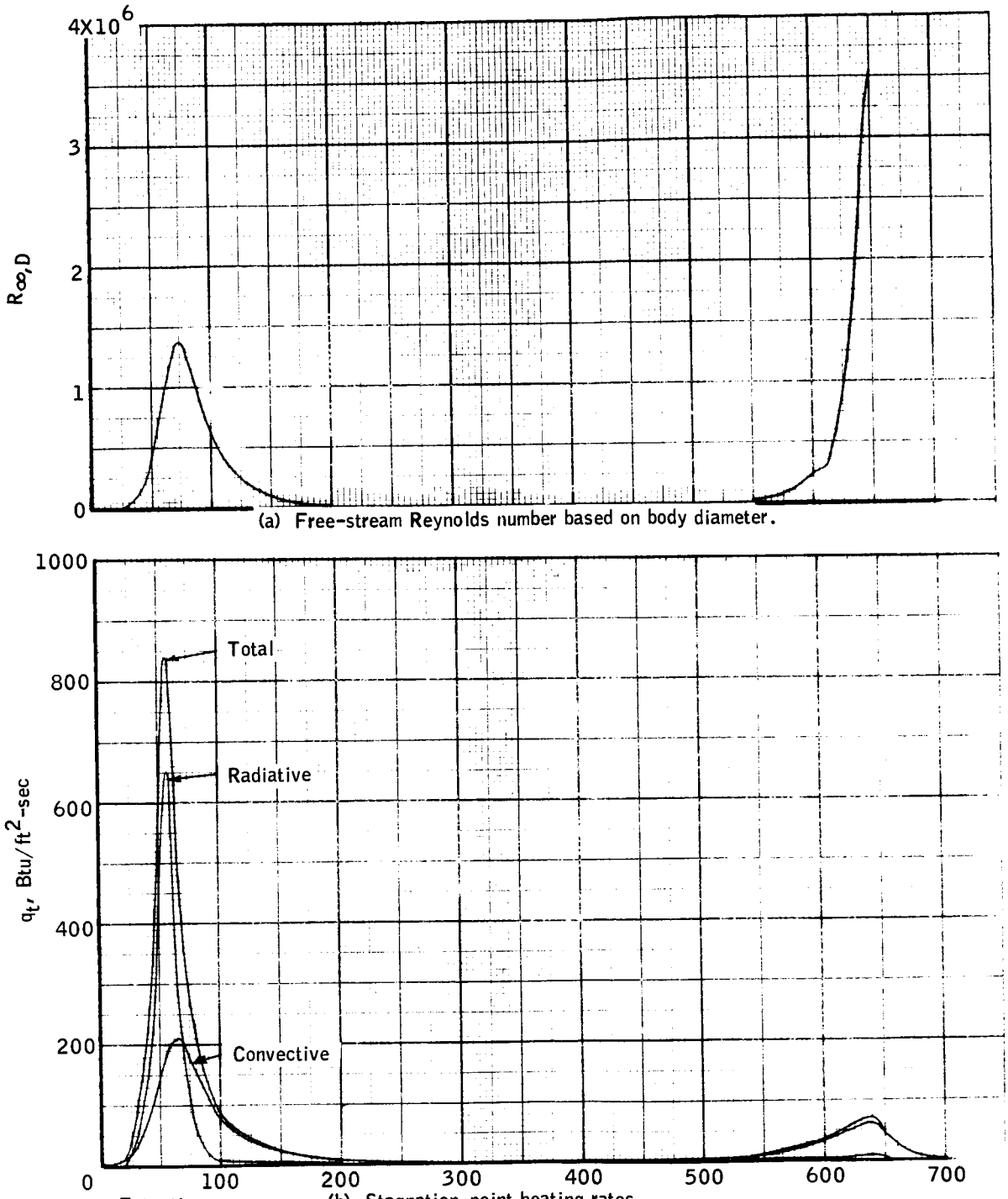

Figure 13.- Free-stream Reynolds numbers and stagnation-point heating rates calculated for heat shield qualification trajectory.

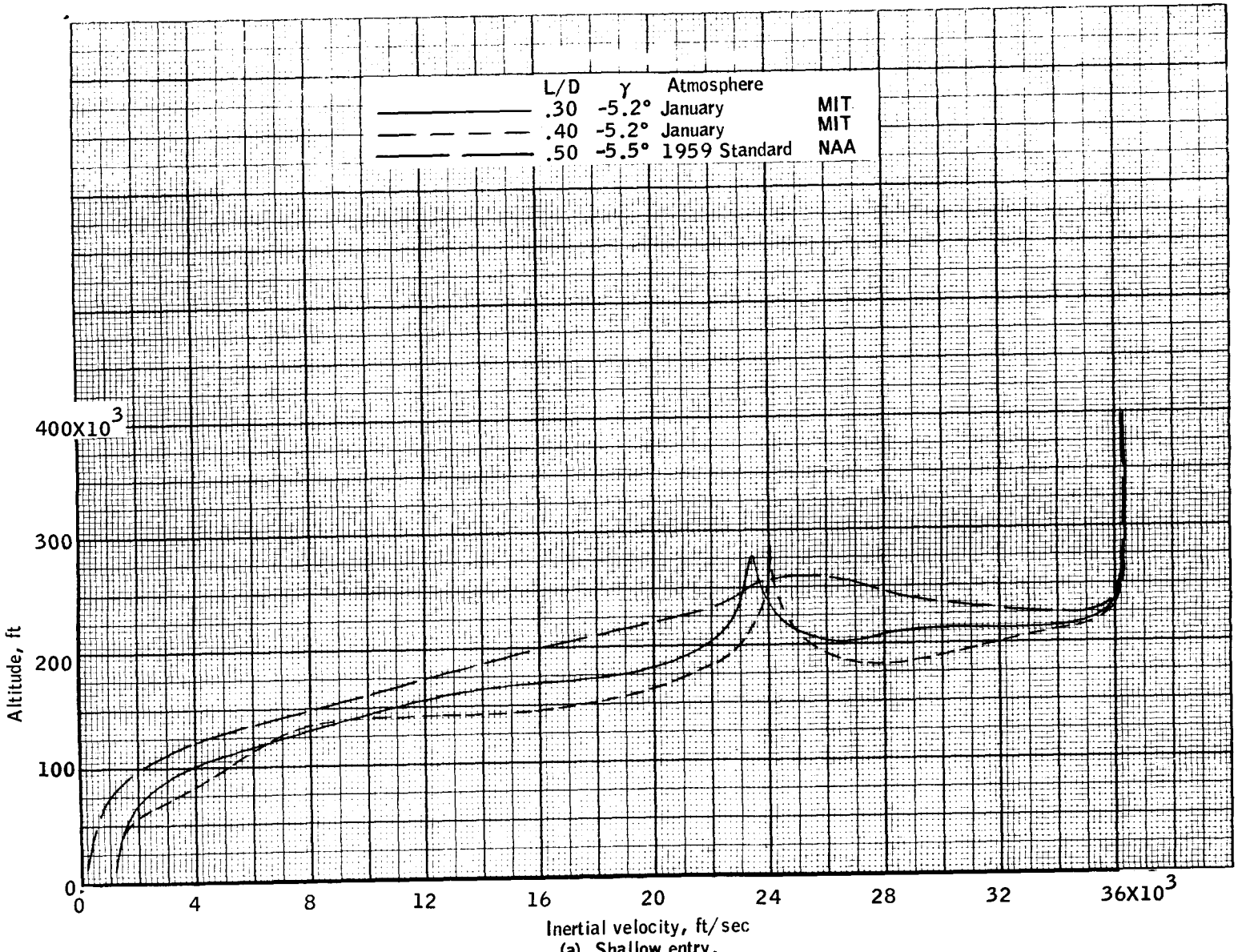

(a) Shallow entry.

Figure 14.- Comparison of NAA trajectories with MSC trajectories using MIT guidance.

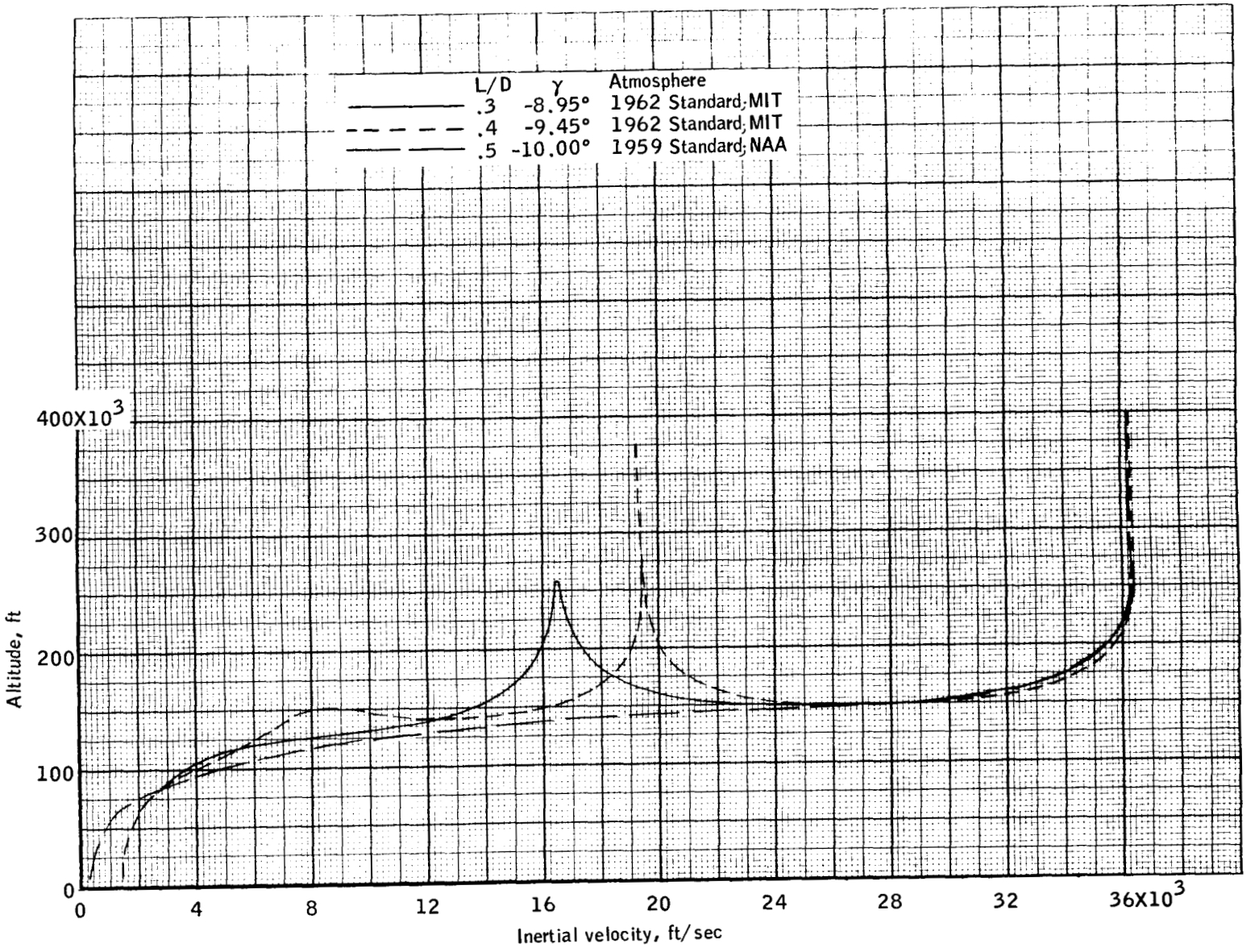

(b) 20 G emergency entry.

Figure 14.- Concluded.

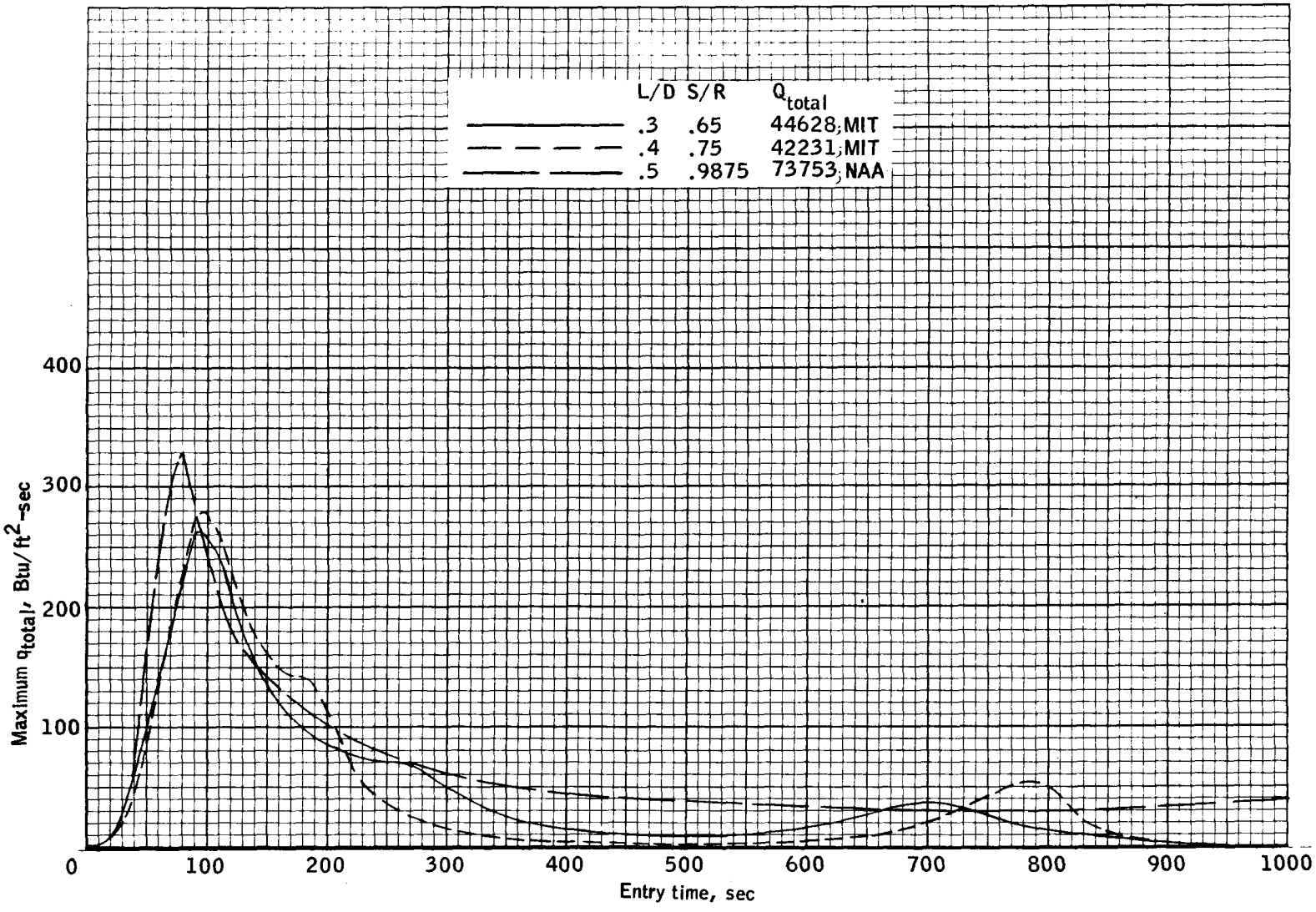

(a) Shallow entry.

Figure 15.- Time histories of maximum heating rates for NAA and MSC trajectories.

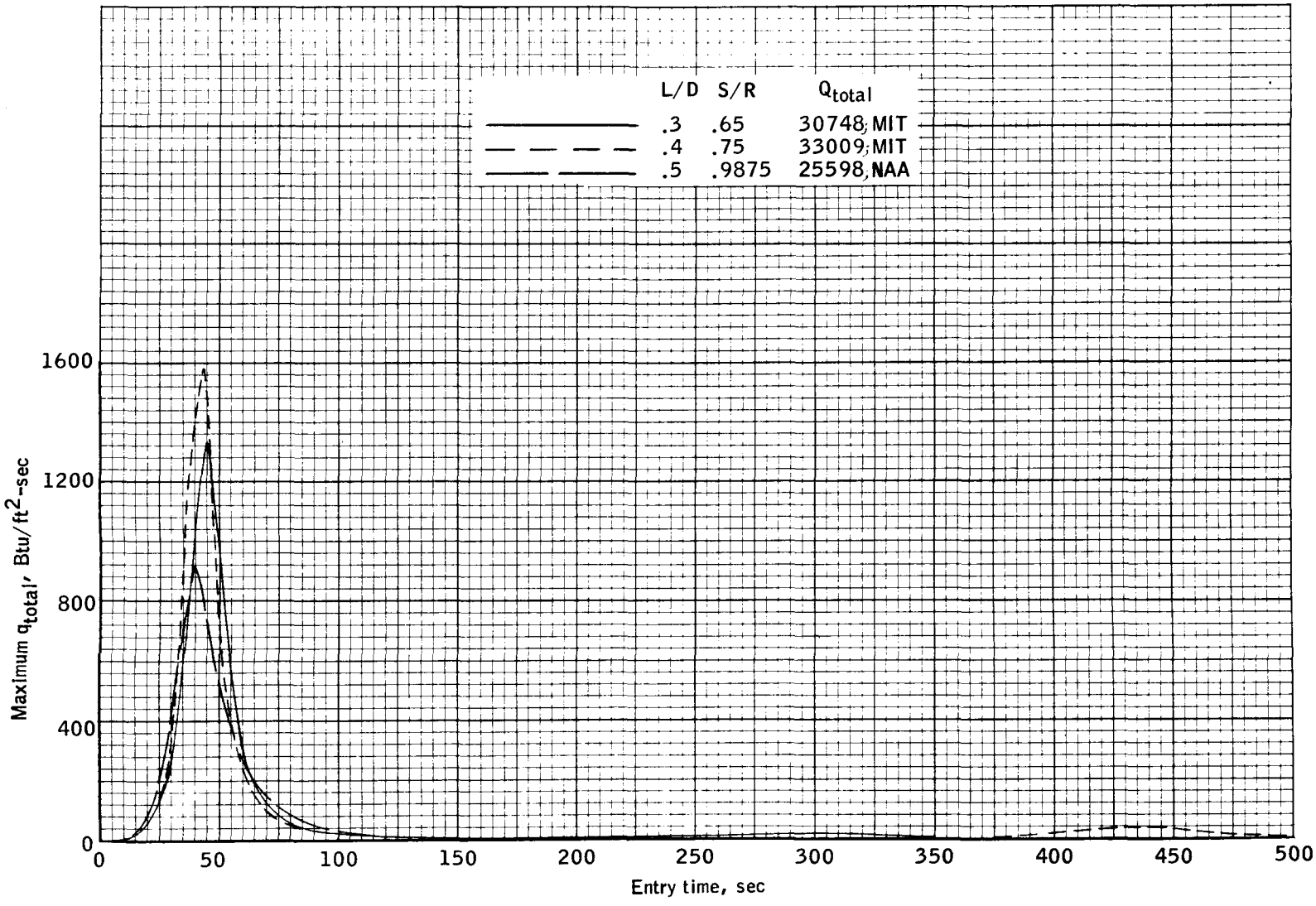

(b) 20 G emergency entry.

Figure 15.- Concluded.